Pergamon

Geochimica et Cosmochimica Acta, Vol. 67, No. 20, pp. 3791–3802, 2003

0016-7037/03 $30.00 + .00

doi:10.1016/S0016-7037(03)00087-5

Competition between iron- and carbon-based colloidal carriers for trace metals in a freshwater assessed using flow field-flow fractionation coupled to ICPMS

BENNY LYVÉN,[1] MARTIN HASSELLÖV,[2] DAVID R. TURNER,[2,*] CONNY HARALDSSON,[1] and KAREN ANDERSSON[2]

[1]Swedish National Testing and Research Institute, P.O. Box 857, SE-501 15 Borås, Sweden
[2]Analytical and Marine Chemistry, Göteborg University, SE-412 96 Göteborg, Sweden

(*Received January* 22, 2002; *accepted in revised form December* 11, 2002)

Abstract—Flow field–flow fractionation (FlFFF) coupled to an inductively coupled plasma mass spectrometer (ICPMS) has been used to determine the chemical composition of colloids from a freshwater sample as a function of size. Organic carbon and iron are the most abundant colloidal components, and are considered as the major carrier phases for other chemical elements present. The size distribution of organic carbon colloids shows a single peak with an estimated hydrodynamic diameter between 1 and 1.5 nm, while the iron colloids show a more complex distribution centred at larger colloid sizes with estimated hydrodynamic diameters up to 5 nm. The association of 32 trace elements with these two carrier colloids has been quantified by deconvolution analysis, and the resulting distributions are shown to be chemically consistent. The observed distributions are also shown to be broadly consistent with predictions from speciation modelling for the subset of 8 elements for which appropriate stability constants are available. *Copyright © 2003 Elsevier Ltd*

1. INTRODUCTION

It is now widely accepted that colloidal material (size range 1 nm–1 μm) plays a significant role in the transport and cycling of trace metals in natural waters (McCarthy and Zachara, 1989; Buffle and Leppard, 1995a; 1995b; Gustafsson and Gschwend, 1997; Lead et al., 1997; Kersting et al., 1999). However, physicochemical characterisation of this material is hampered by a lack of appropriate analytical techniques. Present knowledge of natural water colloids is largely based on physical separation techniques, of which cross flow ultra-filtration is currently widely used to provide concentrates of bulk colloidal material for further analysis (Guo et al., 2000b) This approach does not, however, address the key problem of size distribution and heterogeneity in chemical composition. An additional problem encountered in the study of colloidal material is its instability: natural water colloids are at best in a dynamic steady-state with respect to dissolved and particulate material and to each other (Lead et al., 1997). Analysis techniques based on prior extraction and/or preconcentration of colloids are therefore open to artefacts, most particularly in respect of colloid aggregation and subsequent chemical reaction (Burba et al., 1998). There is thus an urgent need for size fractionation and analysis techniques for colloidal material where the pretreatment is as mild and as rapid as possible (Buffle and Leppard, 1995a; Gustafsson and Gschwend, 1997; Lead et al., 1997). A technique with good potential in this respect is field-flow fractionation (FFF), in which colloids are separated according to their ability to diffuse against a field perpendicular to the carrier flow: the smallest colloids have the fastest diffusion rates and are eluted first (Beckett and Hart, 1993). The most appropriate FFF technique for smaller colloids (1–50 nm) is flow FFF (FlFFF) in which a cross flow provides the perpendicular field in the separation column (Beckett and Hart, 1993; Giddings, 1993). FlFFF, with a flow-through UV absorption detector connected to the channel output, has been used to characterise the size distribution of humic substances isolated (solid phase extraction, XAD-8) from natural waters (Beckett et al., 1987). We have previously shown that colloids from dilute samples can be quantitatively preconcentrated from large injection volumes in a rapid (~30 min) on-channel procedure using a counter-flow focusing technique (Lyvén et al., 1997). This procedure aimed to minimise artefacts associated with the extraction of colloidal material from natural water samples by lowering the preconcentration, and minimising the total analysis time and number of changes in the sample environment. In this work we have used ICPMS as an on-line detector for FlFFF, the multi-element analytical capability of the ICPMS allowing us to determine elemental composition as a function of colloid size within 90 min.

2. EXPERIMENTAL SECTION

2.1. Sampling and Filtration

The freshwater samples were taken in November 1998 from Delsjö Creek (Göteborg, Sweden), a small creek with moderate colloid concentrations (~5 mg L^{-1}). The samples were collected in precleaned polyethylene bottles, and transported to the laboratory, where large particles were removed by filtration through a precleaned 0.45-μm cellulose acetate filter (Millipore). Great care has to be taken when filtering samples since there is always the risk of aggregation or changes in the colloids as well as contamination (Chen and Buffle, 1996a, 1996b). Previous studies (Lyvén et al., 1997) comparing filtration with removal of particles by settling showed no difference in colloidal size or metal distribution between the two pretreatments. Although pretreatment such as filtration is preferably avoided, it is necessary to remove particles > 0.45 μm since they would otherwise cause steric interferences in the FlFFF separation, eluting together with smaller colloids (Myers and

* Author to whom correspondence should be addressed (david@amc.gu.se).

Table 1. Operating conditions for the FIFFF-ICPMS system.

Channel flow (mL min^{-1})	0.50
Cross flow (mL min^{-1})	2.96
Dilution pump flow (mL min^{-1})	1.00
Split ratio (waste:ICPMS)	0.8:0.7
Sample volume (mL)	46.8
Sample load and focusing time (min)	20
UV detector wavelength (nm)	270
ICPMS nebuliser flow (L min^{-1})	0.72
ICPMS auxiliary flow (L min^{-1})	0.8
ICPMS cool gas flow (L min^{-1})	15
RF power (W)	1300

Giddings, 1982). The filtered samples were kept at 4°C and analysed as soon as possible.

2.2. Instrumental

The FlFFF-ICPMS system setup and operating procedure has previously been described in detail in a separate publication (Hassellöv et al., 1999). A quantitative on-channel preconcentration procedure was used to enable the injection of large FlFFF sample volumes (50 mL) (Lyvén et al., 1997). The FFF channel comprises an accumulation wall membrane and a thin mylar spacer clamped between two PMMA (polymethylmethacrylate) blocks. The accumulation wall consists of an ultrafilter membrane (1 kDa MWCO, Omega, PALL-Filtron). The outlet of the FlFFF is connected to a quadrupole ICPMS (VG-PQ 1 upgraded with new electronics and the PQ 2+ interface). The entire system has been made metal-free, and trace-metal clean techniques have been employed to avoid metal contamination; see Hassellöv et al. (1999) for details. The FlFFF carrier (5 mmol L^{-1} borate buffer pH 8.1 + 10 mmol L^{-1} $NaCl^{-}$) has been optimised to resemble the natural chemical environment (ionic strength ~5 mmol L^{-1}) and to be compatible with the demands of both the FlFFF separation and the ICPMS with respect to ionic strength and pH. At the FlFFF-ICPMS interface the FlFFF outflow is mixed (1:2 ratio) with 0.1 mol L^{-1} nitric acid containing indium as internal standard. The threefold dilution of the FlFFF carrier reduces the amount of buffer salt reaching the ICPMS, enabling the instrument to be run an entire day without loss in performance. The nitric acid (final concentration 0.07 mol L^{-1}) helps to solubilise trace metals before introduction to the nebuliser. The operating conditions for the FlFFF and ICPMS are listed in Table 1, and the detection limits and the ratios between measured concentration and detection limit are shown in Table 2.

2.3. Elemental Quantification

The signal obtained from the ICPMS was converted to concentration using blanks and standards prepared in the same matrix as the sample, 1.7 mmol L^{-1} borate, 3.3 mmol L^{-1} sodium chloride and 1% (v/v) nitric acid. The blank and standard solutions, together with the acidified, filtered sample, were measured immediately following the fractogram in the same measurement sequence (Fig. 1). The total concentration in the filtered sample was calculated from the standard and filtered sample responses at the end of the run. The concentration versus retention time curve (fractogram) was integrated to give a total peak area, which was then used, together with the filtered sample response, to calculate the fraction of colloidal metal (i.e., the fraction measured in the integrated fractogram), taking into account the volume injected, the sample split and dilution between the FlFFF and ICPMS, and the ICPMS nebu-

Table 2. Detection limits and ratio between measured concentration and detection limits for selected elements.

Element	Isotope (m/z)	Detection limit[a] (nmol L^{-1})	Measured Concentration[b] / Detection Limit
C	12	c	144[d]
Mg	26	7.7	21
Al	27	11	47
Ca	44	23	91
Mn	55	0.1	31
Fe	57	14	1000
Co	59	0.02	13
Ni	60	0.2	36
Cu	65	1.5	9
Zn	66	0.9	11
Sr	88	0.005	44
Y	89	10	66
Zr	90	1	3
Mo	95	0.1	7
Sb	121	0.1	5
Ba	137	0.3	28
La	139	0.06	111
Ce	140	0.2	41
Pr	141	0.06	34
Nd	147	0.07	18
Gd	157	0.04	17
Dy	162	0.04	23
Pb	208	0.05	52
Th	232	0.03	26
U	238	0.03	18

[a] Determined as 3 times standard deviation of 10 blank runs over a 3-d period.
[b] Sample from Delsjöbäcken, Göteborg using a 46.8-mL sample loop.
[c] Not quantified by ICPMS.
[d] Estimated using 10 times standard deviation of baseline and the fractionated Delsjöbäcken sample.

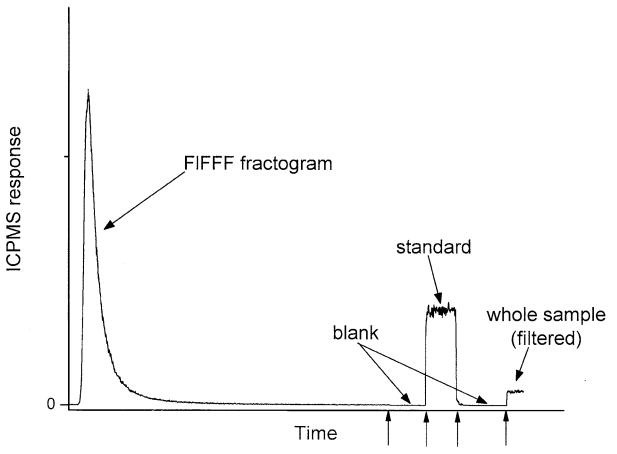

Fig. 1. Elemental quantification sequence in FlFFF-ICPMS. Vertical arrows indicate switching of the ICPMS input stream.

liser flow rate. Organic carbon was quantified by high temperature catalytic oxidation since the carbon signal obtained by ICPMS could not be reliably quantified.

2.4. Enriched Isotope Additions

Following additions of the isotopes ^{63}Cu and ^{206}Pb in acid solution, the pH was adjusted back to natural pH using sodium hydroxide. The samples were allowed to equilibrate with the isotopic spike for 12 h at 4°C before analysis. The isotope additions were not used for quantification nor for mass balance studies, but to verify that the added isotope showed the same size distribution as the metal naturally present. This was done using the ^{63}Cu/^{65}Cu and ^{206}Pb/^{208}Pb ratios.

2.5. Size and Molecular Weight Distributions

The raw fractograms (UV absorbance at 270 nm or trace metal concentration as a function of the retention time), were converted into frequency distributions against size or apparent molecular weight. Size was estimated as the hydrodynamic diameter distribution calculated from FlFFF theory, using a channel volume estimated from void volume and breakthrough measurements. According to FlFFF theory the Stokes (hydrodynamic) diameter, d, can be calculated from retention time t_r, and channel void time t^0 according to

$$d = \frac{2kTbLt_r}{t^0 w \dot{V}_c \eta \pi} \quad (1)$$

where w is the thickness, b the width and L the length of the channel, $\dot{V}_c$ is the volumetric crossflow rate, k is Boltzmann's constant, T the temperature, and η the buffer viscosity.

Molecular weights M_w were estimated from calibration with polystyrene sulphonate (PSS) standards using the equation

$$\log D = -\beta \log M_w + \log \alpha \quad (2)$$

where D is the diffusion coefficient and α and β are calibration constants. This calibration assumes implicitly that the natural colloids have similar characteristics to the PSS standards, and is therefore less appropriate to larger, mineral-dominated colloids. FlFFF theory relates D to the retention parameter λ which describes the thickness of the "cloud" of colloids whose concentration c decreases exponentially from the accumulation wall ($x = 0$):

$$c = c_0 \exp(-x/l) \quad (3)$$

$$\lambda = l/w. \quad (4)$$

D can then be calculated from λ using Eqn. 3 and 4:

$$\frac{t^0}{t_r} = 6\lambda\left[\coth\frac{1}{2\lambda} - 2\lambda\right] \quad (5)$$

$$D = \lambda\frac{\dot{V}_c}{bL}(w). \quad (6)$$

2.6. Reagents

All buffer reagents used were of analytical grade dissolved in Milli-Q water (Millipore). Metal standards were prepared by dilution of 1000 mg L^{-1} stock standard solutions (Merck). High purity acid was prepared in a clean laboratory by sub-boiling point quartz distillation of analytical grade HNO_3 (Merck). The PSS molecular weight standards used (Phenomenex, Torrance, CA, USA; molecular weights 1100, 13,000, 150,000 and 356,000) were dissolved in the FlFFF buffer.

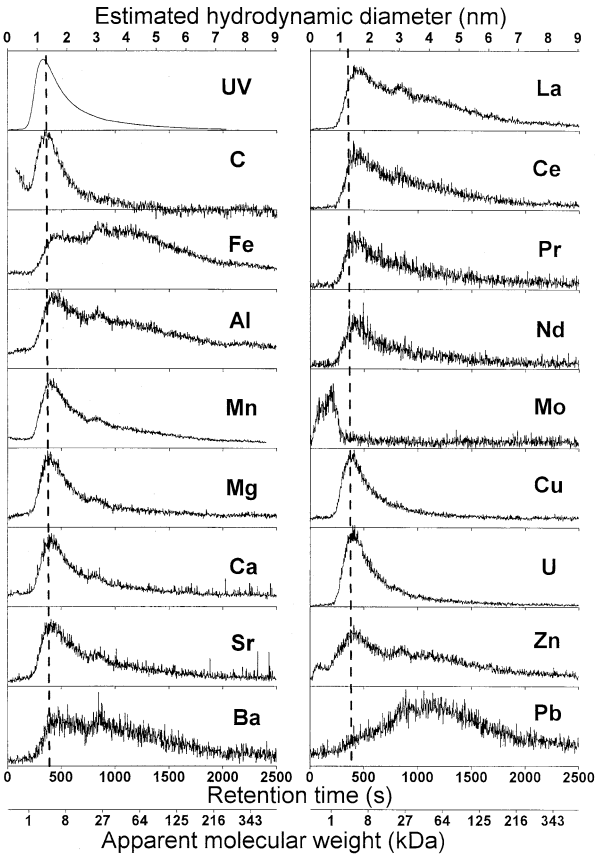

Fig. 2. FlFFF-ICPMS fractograms for selected elements in colloidal material from Delsjö creek, Göteborg, Sweden. The vertical dashed line marks the peak retention time of carbon.

3. RESULTS AND DISCUSSION

3.1. Elemental Colloidal Size Distributions

Using the FlFFF-ICPMS system, the natural colloidal size distributions of 32 different elements have been determined, of which a selection are shown in Figure 2. There are still a number of potentially interesting elements that could not be determined, due to isobaric interferences and/or very low natural concentrations. The most significant of these is silicon, a major component of clay materials that could be used to determine whether or not colloids are of clay origin. In the case of carbon it is important to note that the ability of FlFFF to separate small colloids of the order of 1 nm in size (~1 kDa in molecular weight) means that a significant proportion of the material often classified as dissolved organic carbon (DOC, i.e., the organic carbon passing a 0.45-μm filter) is included here in the colloidal fraction. The size range of this fraction, and its strong fluorescence response (not shown) suggest that it in-

cludes a significant component of humic substances, although lower molecular weight humic substances are expected to pass through the accumulation wall membrane during the focusing step (on-channel preconcentration).

Here we focus first on carbon and iron, which have by far the highest measured colloidal concentrations, and are therefore treated as the most important potential carriers for other elements. The size distributions of iron and carbon are very different: while carbon shows a single colloidal peak, iron has a more complex distribution centred on longer retention times. Although this does not rule out the existence of colloids in the overlap region containing both carbon and iron, it is clear that carbon and iron show very different size distributions, and can therefore be treated as representing competing carrier phases for colloidal trace metals. Several studies, e.g., (Hunter and Liss, 1979; Tipping, 1981), have shown that a surface layer of natural organic matter (NOM, i.e., fulvic or humic acid), which will strongly affect the colloids' surface properties, easily covers iron colloids. While our data neither support nor rule out the presence of a surface layer of NOM on the iron colloids, they do show significant differences in the trace metal content of the carbon- and iron-dominated colloids. We have therefore chosen to focus on the differences between the chemistries of the carbon- and iron-dominated colloids, and have not taken any explicit account of possible absorption of organic species on the iron surfaces.

The carbon fractogram (Fig. 2) shows a peak centred at ~1.2 nm estimated hydrodynamic diameter. This is broadly consistent with AFM and TEM studies of humic substances, which have resulted in size estimates of < 2 nm (Lead et al., 1999) and ≈1 nm (Wilkinson et al., 1999).

3.2. Estimating the Fractionation Between Carbon and Iron Carrier Phases

It is clear from Figure 2 that the two colloidal carrier phases are not fully separated by FlFFF. We describe three different approaches to estimate the proportion of each trace element bound to the carbon and iron carriers respectively. The first is a deconvolution method which has proved to be highly appropriate for this particular dataset, but which is computationally demanding. We therefore also describe two alternative methods of analysis, which are simpler to apply and which may be more appropriate in other systems with a less well-defined distribution between two colloidal populations, and compare the results with deconvolution.

3.2.1. Deconvolution Analysis

Deconvolution analysis involved fitting each FlFFF/ICPMS distribution as the sum of three peaks, which have the form of tailing pulses according to Eqn. 7:

$$\begin{aligned} y &= y_0 \big|_{x < x_0} \\ y &= y_0 + A \times \{1 - \exp[-(x - x_0)/t_1]^{p \times \exp[-(x - x_0)/t_2]}\} \big|_{x \geq x_0} \end{aligned} \quad (7)$$

where y is the signal amplitude, y_0 a constant baseline and x the retention time. Figure 3 shows the deconvolution of the distribution for praseodymium, which is fitted to three peaks P1, P2 and P3. Peaks P1 and P3 are taken to indicate the carbon and iron populations respectively, while peak P2 is a small unidentified peak which occurs in many of the elemental distributions, but whose significance has not been established. The parameters x_0, t_1, t_2 and p were optimised for peaks P1, P2 and P3 using carbon, dysprosium and lead respectively: the optimised parameter values are given in Table 3. These parameters were then used to fit each fractogram to the equation

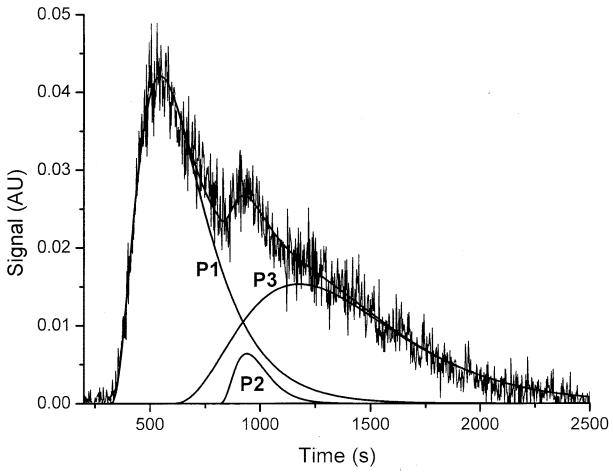

Fig. 3. Deconvolution analysis for praseodymium showing the raw fractogram (dotted line), the three deconvoluted peaks P1, P2 and P3, and the least squares fit to the fractogram (sum of P1, P2 and P3).

$$y = \sum_{i=1,3} y_0^i + \sum_{i=1,3} A^i \times \{1 - \exp[-(x - x_0^i)]/t_1^i]^{p^i \times \exp[-(x - x_0{}^i)/t_2{}^i]}\} \big|_{x \geq x_0}. \quad (8)$$

The results are presented in Table 4, and the calculated distributions of trace elements between carbon and iron colloids are plotted against atomic number in Figure 4.

3.2.2. Retention Time Corresponding to the Element's First FlFFF Peak

The great majority of the measured elements have a first size distribution peak close to that of carbon, but with differences in peak retention time which arise from the combination of two colloidal populations. These small shifts in peak retention time of the first population are used as a measure of the relative amount of material in the two peaks: the larger the apparent peak retention time the greater the proportion of the element bound to iron, which occurs predominantly in a larger size range.

Table 3. Fitting parameters for deconvolution analysis of the fractograms.

Peak	x_0	t_1	t_2	p
P1	290	500	97	2.7
P2	500	350	553	2.7
P3	810	100	87	2.7

Table 4. Metal concentrations, and distribution of colloidal metal calculated by deconvolution analysis.

Element	Total < 0.45 μm (nmol L^{-1})	Total colloidal (nmol L^{-1})	% fractogram assigned to peaks P1, P2 and P3			% fractogram area explained by peaks P1, P2 and P3
			Peak P1 (carbon)	Peak P2	Peak P3 (iron)	
C			100	0	0	99.2
Mg	82,100	166	76	3.5	21	99.9
Al	4450	523	51	2.2	46	99.4
Ca	189,000	2070	74	4.4	22	96.8
Mn	250	3.4	70	3.1	27	100.8
Fe	15,800	14,100	30	1.9	68	100.2
Co	3.16	0.22	87	3.6	9	99.1
Ni	50.6	6.1	92	1.6	6	99.5
Cu	34.0	13.5	88	2.5	9	100.7
Zn	79.1	9.9	64	0.3	36	96.7
Sr	26.3	0.20	71	2.7	26	98.4
Y			68	2.6	29	99.3
Zr			83	2.9	14	99.4
Sb	1.51	0.44	91	0	9	95.5
Ba	164	8.1	54	3.0	44	100.5
La	8.48	7.2	55	2.3	43	100.6
Ce	10.3	8.9	58	2.4	40	101.0
Pr	2.17	1.94	54	3.6	43	100.1
Nd	1.64	1.25	60	2.4	38	100.2
Sm			56	3.1	42	98.2
Eu			57	0.7	42	102.1
Gd	1.68	0.76	63	1.7	35	98.9
Dy	1.44	0.84	66	2.8	31	99.7
Ho	0.25	0.18	66	2.6	32	99.8
Er			71	2.3	27	100.6
Tm			75	1.1	24	97.1
Yb			70	3.4	27	101.1
Lu			71	2.7	26	98.9
Pb	3.0	2.5	13	1.7	85	99.2
Th	1.66	0.80	70	5.0	25	100.6
U	0.55	0.46	84	2.6	13	100.4

3.2.3. *Peak Area Measured Using a Specific Retention Time as Cut-Off*

This approach is similar to using the apparent peak diameter but instead of using a single point, the area under the fractograms (Fig. 2) is divided at a specific diameter; all material smaller than this cut-off diameter taken to represent organic carbon colloids, and all larger material taken to represent iron colloids. The cut-off retention time of 800 s was selected as the valley between the first two peaks of the iron distribution.

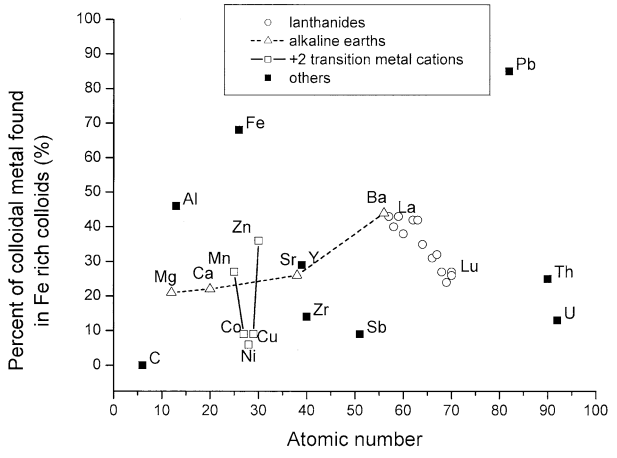

Fig. 4. Percentage of elements found in peak P3 (iron colloids) as a function of atomic number.

3.2.4. *Comparison of the Three Approaches*

We have compared the percentage of colloidal metal associated with the first peak as assessed by the three different approaches. There is a fairly good correlation between deconvolution analysis and area with fixed cut-off ($r = 0.97$): the most significant differences reflect underestimation using the cut-off method. This is especially true for lead and iron, which have the lowest percentages in the first peak. The correlation between deconvolution and peak retention time is poorer ($r = 0.88$) with no trend in the difference between the results. Similar results were also seen if the relative order of the elements for the three models is compared; correlations between deconvolution and area with fixed cut-off ($r = 0.96$) are better than the correlation between deconvolution and peak retention time ($r = 0.86$). Thus we find good agreement between the two methods (deconvolution and fixed cut-off), which use the full fractogram to assess the distribution between the two carriers, and conclude that these give the more reliable estimates in this case.

3.3. Fractionation Between Carbon and Iron Carrier Phases: Discussion

We have shown that three different methods for estimating the fractionation of trace elements between carbon- and iron-dominated colloids are consistent with one another, but are these distributions consistent with the elements' chemistry? Three series of elements marked on Figure 4 provide strong support: these are the alkaline earth elements, the lanthanides, and the +2 cations of the first transition series. The smaller alkaline earth and lanthanide elements show a clear tendency towards higher proportions in the organic carbon colloids than the larger ions. These cations are all (a)-type (Turner et al., 1981), where electrostatic binding dominates over covalent, and it is therefore reasonable that the smaller cations in each series associate with strongly negatively charged organic (humic) colloids in preference to iron colloids which have a small positive charge at the sample pH (≈6.5) (Dzombak and Morel, 1990; Stumm and Morgan, 1996). Although adsorption of organic matter would result in a negative surface charge on the iron colloid surface, the negative charge density would be significantly less than that at purely humic colloids, so that a significant difference in electrostatic binding would still be expected. The cations of the first transition series, which show only small variations in ionic radius, follow the well-known Irving-Williams series where complex formation (in this case association with organic colloids) is least for Mn and Zn, and highest for Co, Ni and Cu (Phillips and Willliams, 1966). In marine waters, where the colloids are dominated by organic carbon, Guo et al. (2000a) also found an Irving-Williams dependence of metal-carbon colloid association.

One element not shown in Figure 4 is molybdenum, which elutes before the carbon peak (Fig. 2). This is interpreted as elution of the dissolved molybdate ion, which is not associated with colloids but evenly distributed across the channel thickness, and which therefore elutes as a void peak with the first channel volume. This is consistent with thermodynamic predictions of Mo speciation (Turner et al., 1981), and with previous observations in a nearby river that Mo is retained by DEAE resin but not by Chelex (Haraldsson et al., 1993). Although the molybdate ion is smaller than the accumulation wall membrane's nominal cut-off (1 kDa), these cut-off values are determined for globular proteins, and the diffusion of the molybdate anion through pores in a negatively charged membrane can be much slower than expected from the molecular weight. In addition, the relatively short contact time between sample and membrane results in a effective cut-off smaller than the membrane's nominal pore size (Guo et al., 2000b). Other oxyanions could be expected to behave similarly, but most of these could not be measured in this work due to isobaric interferences, concentrations below detection limits, and/or loss of the small oxyanions through the FlFFF accumulation wall membrane. Antimony, which is also predicted to be present in anionic form as $Sb(OH)_6^-$ at this pH (Turner et al., 1981) is, however found mainly associated with organic carbon colloids, which may indicate formation of organic complexes. The small fraction of zinc eluting before the organic colloids cannot at present be explained.

In contrast to the oxyanions, uranium forms the oxocation UO_2^{2+} at equilibrium in oxic waters: this cation is known to have a very strong affinity for carbonate ions (Turner et al., 1981). While carbonate concentrations are very low in the near-neutral freshwater studied, binding to carboxylate groups in humic substances may contribute to the observed association with organic colloids (Fig. 4).

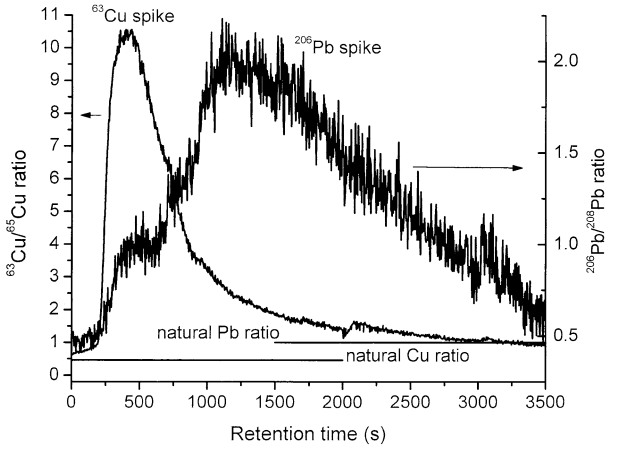

Figure 5. The isotopic ratio of $^{63}Cu/^{65}Cu$ and $^{206}Pb/^{208}Pb$ in a freshwater sample spiked with ^{63}Cu and ^{206}Pb isotopes. Also shown are the natural isotopic ratio for $^{63}Cu/^{65}Cu$ and an approximate ratio for $^{206}Pb/^{208}Pb$.

Only lead was found mainly adsorbed (85%) to the large colloids. The low percentage of Pb in the organic colloids is surprising: Pb is known to have an affinity for natural organic matter in the form of humic substances, although its binding is observed to be somewhat weaker than that of, for example, Cu (Tipping and Hurley, 1992). Our results are, however, consistent with a previous study in a nearby river which found that both dissolved and particulate lead followed the iron concentrations (Danielsson et al., 1983), and with a study in Galveston Bay, USA, which found a strong correlation between colloidal Pb and Fe (Wen et al., 1999). Similar conclusions were drawn by Lofts and Tipping (2000) from a study of metal partitioning in the Humber river system. The sharp difference between the behaviour of Pb and the other +2 cations is intriguing: the very short residence time for Pb in oceanic waters (Whitfield and Turner, 1987) indicates a strong affinity for (larger) sinking particles, but it is at first surprising that Pb is unique in associating only with the larger iron colloids in this sample. To verify that the unique behaviour of Pb reflected adsorption processes rather than matrix-bound Pb, additions of enriched lead (^{206}Pb) and copper (^{63}Cu) isotope material were made to the sample. The resulting isotope ratios are shown in Figure 5: isotopic equilibrium has clearly not been established, so that the distributions of the added isotopes indicate the relative uptake rates of the added metals by the two colloid carriers. The results show that the copper and lead spikes have been taken up most rapidly by the carbon and iron colloids respectively, reflecting the equilibrium distributions shown in Figure 2.

3.4. Speciation Modelling

The identification of carbon- and iron-dominated carrier phases opens the possibility of developing speciation models for colloidal material. As a starting point, we have used existing

speciation models and stability constants for hydrous ferric oxide (Dzombak and Morel, 1990) and humic substances (Tipping, 1994) for the iron and carbon carriers respectively. These models and stability constant compilations have been selected as the most coherent and comprehensive treatments in their respective fields. It is, however, important to be aware that we thus implicitly make a range of assumptions: that the iron colloids have the same properties as the hydrous ferric oxides studied by Dzombak and Morel (1990), that the acid-base and complexation chemistry of organic carbon colloids are dominated by humic materials with the properties represented in Tipping's (1994) model, that trace metals are adsorbed/complexed by the carriers rather than constituting matrix components, and that uptake of trace metals is not affected by any interactions between the iron and organic carbon colloids.

3.4.1. Iron Colloids

The Delsjö Creek sample contained 14.1 μmol L^{-1} colloidal iron. Following Dzombak and Morel (1990), we assume that the iron colloids contain 0.2 mol metal binding sites per mole of iron, and that the surface area is 600 m_2 g^{-1} (assuming the colloid to have the composition FeOOH).

3.4.2. Organic Carbon Colloids

The Delsjö Creek sample contained 4 mg L^{-1} organic carbon. Following Tipping (1996), we take the concentration of humic substances also be to 4 mg L^{-1}. This is based on the assumption that 50% of the carbon is contained in humic substances, and that humic substances contain 50% carbon by weight. Thus we also implicitly assume that the non-humic fraction of the organic carbon does not play any role in complexing or adsorbing trace metals. In Tipping's model, humic substances can be defined either as fulvic or humic acids, with molecular weights of 1500 and 15,000 respectively. Although the molecular weight estimates from FlFFF suggest that the organic carbon colloids measured are closer to fulvic than humic acid in molecular weight, we have modelled using both options to compare the results.

3.4.3. Metals

The compilations of Dzombak and Morel (1990) and Tipping (1994) do not contain binding constants for all of the trace elements measured, and therefore restrict modelling to the doubly charged cations of Ca, Sr, Ba, Co, Ni, Cu, Zn and Pb. The metal concentrations used in the calculations are those given in Table 4 (total < 0.45 μm).

3.4.4. Calculations

We first calculated the distributions of these cations between truly dissolved (inorganic) metal, humic or fulvic bound, and iron-bound (Figs. 6 and 7). The Delsjö Creek water has pH $\approx$ 6.5, but we have calculated distributions in the pH range 5 to 8 to cover the pH range typical of fresh waters in southwest Sweden. We can see that iron colloids play only a minor role at pH 5 but an increasingly important role as the pH increases. The model hydrous ferric oxide has a point of zero change close to pH 8 (Dzombak and Morel, 1990), in contrast to the humic substances with points of zero charge at much lower pH (<3) (Morel and Hering, 1993; Varney et al., 1983), and which are therefore strongly negatively charged at all pH values modelled here. At pH 5, 6 and 7 the binding of the transition metals Co, Ni, Cu and Zn shows a clear Irving-Williams order with copper showing the strongest binding. Lead is modelled to behave very differently from the other metals, being strongly associated with the iron colloids even at pH 7. This is in agreement with the experimental results (above) where lead, uniquely, showed no association with the smaller colloids, binding only to the larger iron colloids. Comparing the distributions calculated for humic and fulvic acids, each results in similar distribution patterns but the humic acid clearly binds the metals more strongly and thus competes somewhat more effectively with the iron colloids.

To compare our model calculations directly with the experimental data, we first calculated the colloidal fraction of each trace metal at pH values 6, 6.5 and 7 (Fig. 8). Throughout this pH range the model tends to overestimate the proportion of metal in colloidal form, but produces a similar Irving-Williams-like distribution pattern, particularly at pH 6 and 6.5. Figure 9 shows the calculated proportion of the colloidal metal associated with iron colloids at the same pH values, together with the experimental estimate obtained from deconvolution analysis of the fractograms (Table 4). Given the number of assumptions made in the modelling and in the interpretation of the fractograms, the degree of agreement shown in Figure 9 is remarkable.

3.4.5. Discussion

The results shown in Figures 6 to 9 have been obtained using a simplified model of the colloidal material in Delsjö Creek water. We have used model parameters and constants obtained form the literature, and made no attempt to optimise the model to fit the experimental data. The formulations and parameters used may, therefore, not be fully appropriate to the Delsjö Creek sample, and neglect of potential organic carbon adsorption onto iron colloids may also cause divergence between experimental data and the modelling results. We can, however, draw encouragement from the model's ability to reproduce key interelement differences in the size of the colloidal faction (Fig. 8) and the distribution between iron- and carbon-based colloids (Fig. 9). Indeed, the marked difference between the observed chemistries of iron- and carbon-dominated colloids (Figs. 2, 4, and 9), together with the ability of this simple modelling exercise to reproduce the major features of these differences, argues against the surface of the iron colloids being fully covered with organic matter, as this would result in similar chemical characteristics for both colloid types.

3.5. Elemental Colloid Size Distributions—Comparison With Literature Data

How well do these results compare with previous investigations? Differences in the natural water samples, together with the much poorer size resolutions of other methods, make quantitative comparison difficult. We have nevertheless thought it worthwhile to attempt a comparison with the available literature data. In Table 5 we have compared our results with

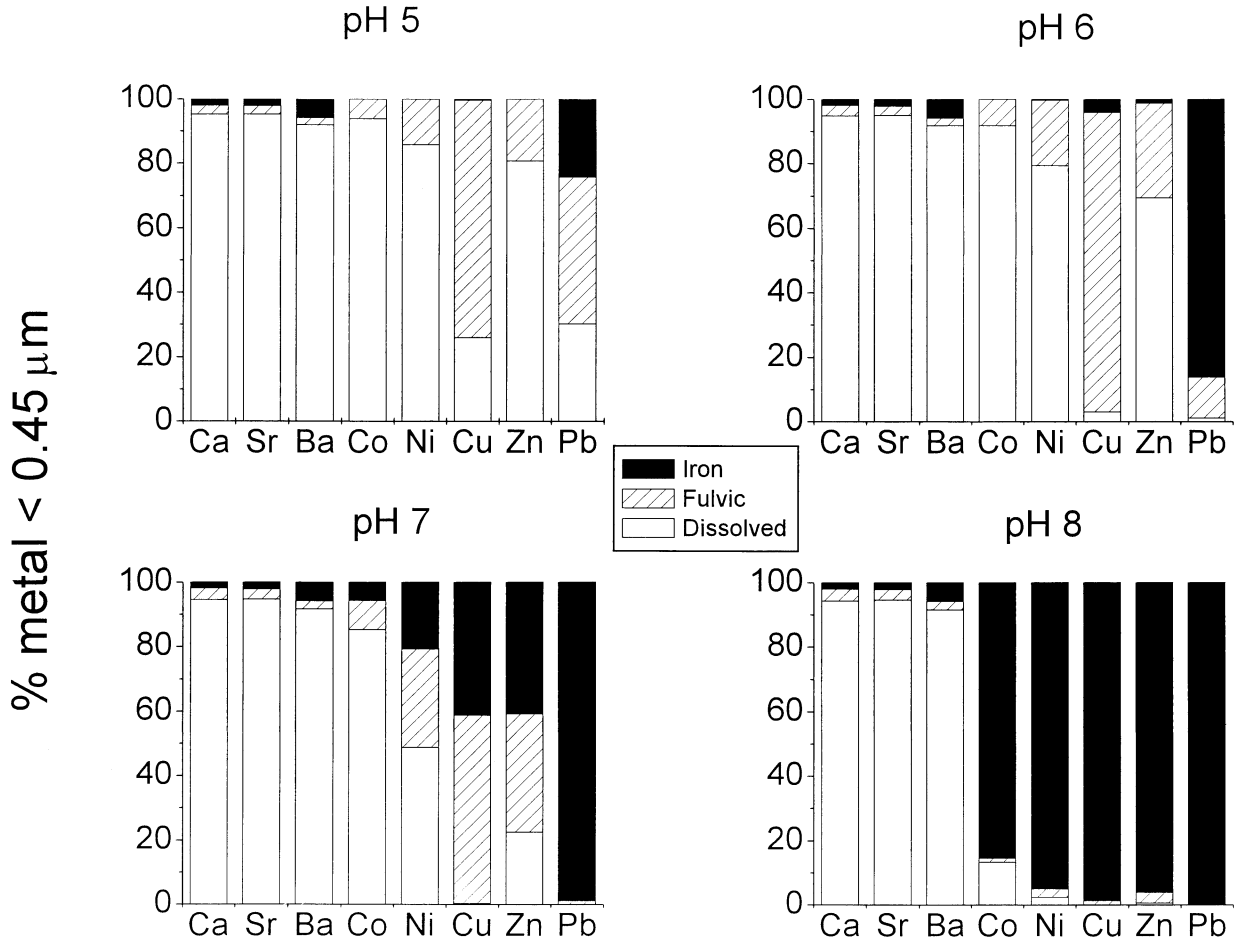

Fig. 6. Modelled distributions of dissolved and colloidal metals using fulvic acid model.

published data on cross-flow ultrafiltration (CFF) of river and lake samples (Hoffmann et al., 1981; Tanizaki et al., 1992; Martin and Dai, 1995; Powell et al., 1996; Pham and Garnier, 1998; Wen et al., 1999), and with coupled SEC-ICPMS analysis of organic matter isolates prepared using XAD-8 extraction or ultrafiltration (Vogl and Heumann, 1997, 1998; Haraguchi et al., 1998). There are numerous results published for colloidal and metal concentrations and a selection was made using data from freshwater samples including the highest number of determined metals.

The range of different molecular weight cutoff values of the ultrafilter membranes used by different workers (1, 3 and 10 kDa are the most common) complicates comparisons with our size distributions. To provide a coherent comparison, we have compiled data for separations at 1 kDa, below which all material is assumed to be truly dissolved, and at 10 kDa, which has been used to distinguish between smaller and larger colloids. Inspection of Figure 2 reveals that the 1- to 10-kDa size class contains the carbon and first iron peaks, while the major fraction of the colloidal iron falls into the larger colloidal size class. Comparing the FlFFF-ICPMS and CFF estimates of the colloidal fraction of "total dissolved" metals (Table 5, columns 2 and 3), we find surprisingly good agreement with the exception of some +2 cations where the FlFFF-ICPMS estimates are very much lower. Comparison between our data and the most consistent CFF dataset, where 39 elements were analysed with neutron activation analysis (Tanizaki et al., 1992), shows a reasonable agreement for the smaller (<1 kDa) and larger (>10 kDa) size fractions, but very poor agreement for the intermediate size fraction. The additional error associated with taking the difference between two CFF separations may be a contributing factor in this poorer agreement in the intermediate size range. It is worth noting here that CFF and FlFFF both make use of ultrafilter membranes; in CFF the membrane is the size separator, while in FlFFF the membrane is used only to retain colloids within the channel, and contact time between the sample and the membrane is considerably shorter than in CFF, which may minimise artefacts due to e.g., membrane adsorption. Both methods can potentially suffer from artefacts due to colloid aggregation (see also section 3.6.2 below); enhanced colloid concentrations in FlFFF are, however, relatively short-lived, occurring only during the focusing stage.

The SEC results (shown in italic in Table 5) are much more limited, but show a similar pattern to the CFF results. Of particular interest is Mo, where we find no evidence of association to organic colloids, in contrast to results reported from SEC-ICPMS measurements on XAD-8 isolated organic material (Vogl and Heumann, 1998): while these differences may

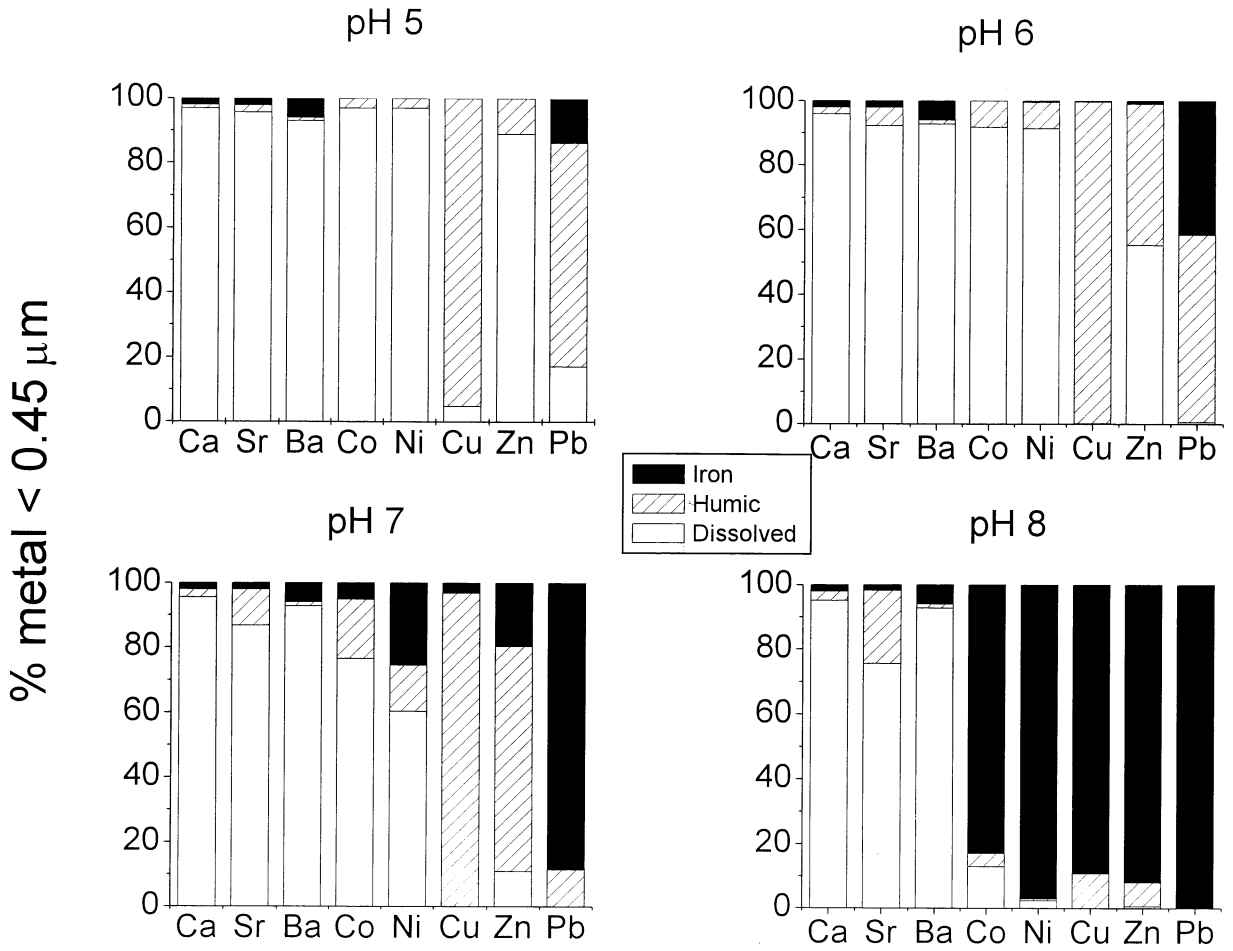

Fig. 7. Modelled distributions of dissolved and colloidal metals using humic acid model.

reflect the different origins of the samples analysed, they may also arise from the very different sample treatments involved. For example, in the case of Mo noted above, the colloidal material was subjected to extensive and harsh pretreatment in the form of adsorption onto an XAD-8 column, elution, and interaction with the SEC column material. The FlFFF-ICPMS sample treatment is much milder and more rapid than SEC, comprising accumulation and separation in the FlFFF channel, which has the form of an open column. It is to be expected that this milder and shorter sample treatment results in fewer artefacts and thus gives a more accurate estimate of the true colloid size distribution.

3.6. Potential Artefacts in the FlFFF Separation

When determining size or molecular weight distributions of natural organic material there is always the possibility of loss of material during analysis, most commonly by adsorption but in this case also by molecules escaping through the accumulation membrane. When carrying out metal determinations on-line with the size fractionation, ion exchange processes and contaminant adsorption may occur, affecting the resulting size distribution and amount of metal found in the colloids. There is also the risk of disturbing the colloids during pretreatment and analysis.

3.6.1. Losses of Material During Analysis

A common way of verifying an analytical procedure is by carrying out a mass balance study. However, when dealing with colloids it is difficult to perform an accurate mass balance, especially when natural concentrations are low and few or no comparable techniques are available. Previous studies, on the organic fraction absorbing UV-light at 270 nm, have shown that the procedure employed here can quantitatively preconcentrate and separate the natural colloids (Lyvén et al., 1997). For the mass balance of trace metals, results obtained from the fractionation of natural samples (Delsjöbäcken) as well as previously published results from the same waters can give some information as to what extent losses could occur. The determination of praseodymium, which has low contamination problems, showed a recovery of 90% of the < 0.45 μm metal in the colloidal fraction, the remaining 10% representing truly dissolved metal and/or losses during the FlFFF separation: any loss is therefore $< 10\%$. Other elements such as Ce, Fe, La, Pb and U also show high colloidal metal recoveries, between 83

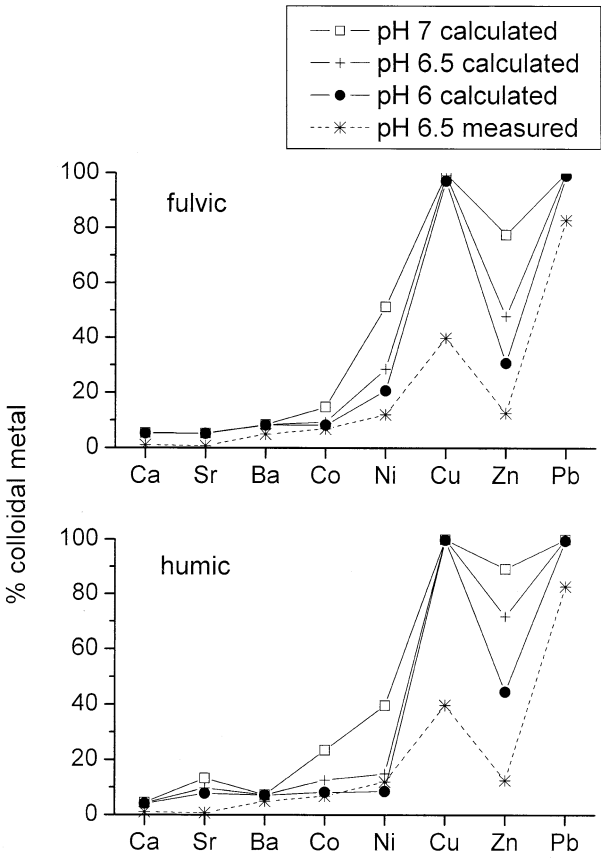

Fig. 8. Modelled and measured fractions of metals in colloidal form.

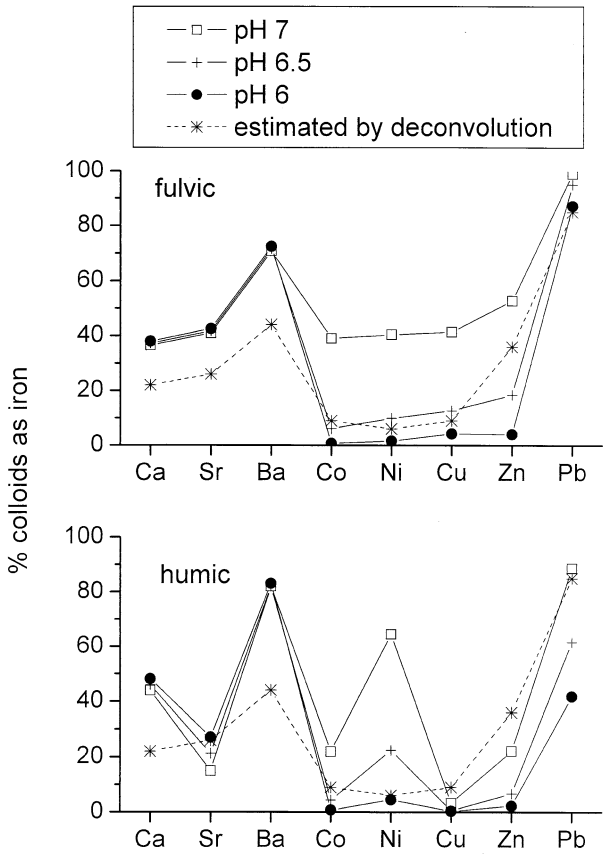

Fig. 9. Modelled fraction of colloidal metals associated with iron, compared with the estimate from deconvolution analysis (Table 4).

and 89%. Previous published results by Haraldsson et al. (1993) for the same water mass showed that 15 to 20% of the lead was found as truly dissolved, which agrees well with the estimate of 83% colloidal lead in this work. Molybdenum, which occurs as an oxyanion, showed very different behaviour with colloidal recoveries of no more than 15%, presumably reflecting a truly dissolved fraction. Potential losses during separation are, however, still a matter of concern, and further mass balance studies are required. This would require additional analyses, determining the truly dissolved fraction, which is often very difficult.

3.6.2. Aggregate Formation and Colloid Adsorption During Analysis

During the loading of large sample volumes, an increasing concentration of colloids occurs within the FlFFF channel, most particularly at the focus point. This results in a colloidal concentration many times (>1000) higher than present in the sample before analysis. This large increase in concentration could cause the colloids to aggregate forming larger colloids. However, if there is an aggregation occurring, the process is very repeatable, resulting in the same size and metal distributions (Hassellöv et al., 1999), even when runs with different crossflows are compared. Previous results (Lyvén et al., 1997) showed that for the first organic, UV-light absorbing peak no change in retention time (i.e., size) could be observed when changing sample volumes between 1.74 and 106 mL, nor when changing sample loading times from 8.5 to 95 min. This suggests that if there is aggregation of the smaller carbon based colloids, it is fast and repeatable.

4. CONCLUSIONS

We have shown that the coupled ICPMS-FlFFF system can be used to determine colloidal and metal distributions in natural waters. The results obtained show that the fresh water analysed contains two major types of colloids, dominated by carbon and iron respectively. The organic carbon colloids have a small size (~1.2 nm) and a narrow size distribution whereas the iron rich colloids peak at a larger size (~4 nm) with a broader size distribution. Three different approaches have been used to determine the fractionation between the colloidal phases. The use of apparent peak diameters and peak area with fixed cut-off gives a rough estimation whereas deconvolution is, at present, the most promising method for estimating the relative importance of carbon versus iron rich colloids.

The studied elements can be divided into four groups with different distribution patterns: (1) dissolved simple anions, (2) elements mainly adsorbed to carbon-based colloids, (3) elements mainly adsorbed to iron-rich colloids, and (4) elements almost equally distributed between the carbon and iron col-

Table 5. Distribution of colloidal material into size classes: comparison of literature data with FIFFF-ICPMS determinations.

	Colloidal Fraction (1kDa–0.45μm) / "Total Dissolved" (<0.45 μm) (%)		Larger Colloids (10 kDa–0.45μm) / Colloidal Fraction (1 kDa–0.45μm) (%)	
	This work (FIFFF-ICPMS)	Literature data (CFF or *SEC*[a])	This work (FIFFF-ICPMS)	Literature data (CFF or *SEC*[a])
C	b	80[c], 72[l], 28[m]	34	73[l], 52[m]
Mg	0.20	29[e], 37[f]	53	5.2[f], 14[e], *1.2*[g]
Al	12	11[e]	77	41[e], *65*[g]
Ca	1.1	20[f], 29[e]	57	7.0[f], 17[e], *1.5*[g]
Mn	1.4	24[h], 30[e], 39[f]	63	38[f], 13[f], 6.0[i], 19[e]
Fe	89	82[g], 91[e], 95[f], 68[i], 95[m]	87	56[f], 55[i], *77*[e], *92*[g], 95[l], 99[m]
Co	6.9	62[e], 4[m]	43	8.1[i], 13[e], 24[m]
Ni	12	8.2[h], *45*[j], 58[e], 30[l], 14[m]	43	9.1[e], 100[i], 35[m]
Cu	40	44[h], *43*[j], 50[l], 22[m]	42	41[f], *70*[g], 89[i], 33[m]
Zn	13	57[e], *15*[j], 51[m]	70	22[e], *95*[g], 53[m]
Sr	0.75	27[e]	63	6.8[e], *3.0*[g]
Y	2.9	d	65	*51*[g]
Zr	5.0	d	50	d
Mo	15[k]	81[j], 100[c]	0	d
Sb	29	26[e]	37	13[e]
Ba	4.9	27[e]	83	17[e], *7.0*[g]
La	85	88[e]	76	46[e], *69*[g]
Ce	86	84[e]	76	70[e], *77*[g]
Pr	90	d	75	*74*[c]
Nd	b	d	73	d
Sm	76	84[e]	71	42[e], *63*[g]
Eu	b	d	69	d
Gd	45	d	70	*52*[g]
Dy	59	d	69	*70*[g]
Ho	71	81[e]	64	31[e], *52*[g]
Er	b	d	64	d
Tm	b	d	65	d
Yb	b	d	62	d
Lu	b	d	61	d
Pb	83	49[h], *100*[j], 57[m]	96	71[m]
Th	48	82[e]	61	77[e]
U	84	66[e]	49	18[e], *31*[g]

[a] SEC-ICPMS involves preconcentration using UF or XAD-8 (solid phase extraction).
[b] Sample concentration not determined.
[c] Vogl and Heumann (1998).
[d] No published results found.
[e] Tanizaki et al. (1992).
[f] Hoffmann et al. (1981).
[g] Haraguchi et al. (1998).
[h] Martin and Dai (1995).
[i] Pham and Garnier (1998).
[j] Vogl and Heumann (1997).
[k] Mo behaves as close to 100% dissolved molybdate, the percentage found is severely affected by losses through the membrane.
[l] Powell et al. (1996).
[m] Wen et al. (1999).

loids. A majority of the studied elements fall into the last of these groups. Limitations in the instrumentation still make it impossible to measure some elements, the most important being silicon, causing some remaining uncertainties in the composition of the colloids. The observed trace metal distributions are consistent with the predictions of a highly simplified colloidal speciation model.

Acknowledgments—This work was supported by grants from the Swedish Natural Science Research Council and Göteborg University Marine Research Centre. We thank Bill Landing and three anonymous reviewers for their thorough and constructive reviews of the original manuscript.

Associate editor: R. H. Byrne

REFERENCES

Beckett R. and Hart B. T. (1993) Use of field-flow fractionation techniques to characterise aquatic particles, colloids, and macromolecules. In *Environmental Particles, Vol. 2* (eds. J. Buffle and H. P. van Leeuwen), pp. 165–205. Lewis Publishers.

Beckett R., Jue Z., and Giddings J. C. (1987) Determination of molecular weight distributions of fulvic and humic acids using flow field-flow fractionation. *Environ. Sci. Technol.* **21,** 289–295.

Buffle J. and Leppard G. (1995a) Characterization of aquatic colloids and macromolecules. 1. structure and behavior of colloidal material. *Environ. Sci. Technol.* **29,** 2169–2175.

Buffle J. and Leppard G. (1995b) Characterization of aquatic colloids and macromolecules. 2. Key role of physical structures on analytical results. *Environ. Sci. Technol.* **29,** 2176–2184.

Burba P., Aster B., Nifant'eva T., Sckinev V., and Spivakov B. Y. (1998) Membrane filtration studies of aquatic humic substances and

their metal species: A concise overview. Part 1. Analytical fractionation by means of sequential-stage ultrafiltration. *Talanta* **45,** 977–988.

Chen Y. W. and Buffle J. (1996a) Physicochemical and microbial preservation of colloid characteristics of natural water samples. 1. Experimental conditions. *Water Res.* **30,** 2178–2184.

Chen Y. W. and Buffle J. (1996b) Physicochemical and microbial preservation of colloid characteristics of natural water samples. 2. Physical and microbial evolution. *Water Res.* **30,** 2185–2192.

Danielsson L.-G., Magnusson B., Westerlund S., and Zhang K. (1983) Trace metals in the Göta river estuary. *Est. Coastal Shelf Sci.* **17,** 73–85.

Dzombak D. A. and Morel F. M. M. (1990) *Surface Complexation Modelling: Hydrous Ferric Oxide*. John Wiley, New York.

Giddings J. C. (1993) Field-flow fractionation: Analysis of macromolecular, colloidal, and particulate matter. *Science* **260,** 1456–1465.

Guo L., Santschi P. H., and Warnken K. W. (2000a) Trace metal composition of colloidal organic material in marine environments. *Mar. Chem.* **70,** 257–275.

Guo L., Wen L.-S., Tang D., and Santschi P. H. (2000b) Re-examination of cross-flow ultrafiltration for sampling aquatic colloids: Evidence from molecular probes. *Mar. Chem.* **69,** 75–90.

Gustafsson Ö. and Gschwend P. M. (1997) Aquatic colloids: Concepts, definitions and current challenges. *Limnol. Oceanogr.* **42,** 519–528.

Haraguchi H., Itoh A., Kimata C., and Miwa H. (1998) Speciation of yttrium and lanthanides in natural water by inductively coupled plasma mass spectrometry after preconcentration by ultrafiltration and with a chelating resin. *Analyst* **123,** 773–778.

Haraldsson C., Lyvén B., Pollak M., and Skoog A. (1993) Multielement speciation of trace metals in fresh water adapted to plasma mass spectrometry. *Anal. Chim. Acta* **284,** 327–335.

Hassellöv M., Lyvén B., Haraldsson C., and Sirinawin W. (1999) Determination of continuous size and trace element distribution of colloidal material in natural water by on-line coupling of flow field-flow fractionation with ICP-MS. *Anal. Chem.* **71,** 3497–3502.

Hoffmann M. R., Yost E. C., Eisenreich S. E., and Maier W. J. (1981) Characterization of soluble and colloidal-phase metal complexes in river water by ultrafiltration. A mass-balance approach. *Environ. Sci. Technol.* **15,** 655–661.

Hunter K. A. and Liss P. S. (1979) The surface charge of suspended particles in estuarine and coastal water. *Nature* **282,** 823–825.

Kersting A. B., Efurd D. W., Finnegan D. L., Rokop D. J., Smith D. K., and Thompson J. L. (1999) Migration of plutonium in ground water at the Nevada Test Site. *Nature* **397,** 56–59.

Lead J. R., Davison W., Hamilton-Taylor J., and Buffle J. (1997) Characterizing colloidal material in natural waters. *Aquat. Geochem.* **3,** 212–232.

Lead J. R., Balnois E., Hosse M., Menghetti R., and Wilkinson K. J. (1999) Characterization of Norwegian natural organic matter: Size, diffusion coefficients, and electrophoretic mobilities. *Environ Intern.* **25,** 245–258.

Lofts S. and Tipping E. (2000) Solid-solution metal partitioning in the Humber rivers: Application of WHAM and SCAMP. *Sci. Tot. Environ.* **251–252,** 381–399.

Lyvén B., Hassellöv M., Haraldsson C., and Turner D. R. (1997) Optimisation of on-channel preconcentration in flow field-flow fractionation for the determination of size distributions of low molecular weight colloidal material in natural waters. *Anal. Chim. Acta* **357,** 187–196.

Martin J.-M. and Dai M.-H. (1995) Significance of colloids in the biogeochemical cycling of organic carbon and trace metals in the Venice Lagoon (Italy). *Limnol. Oceanogr.* **40,** 119–131.

McCarthy J. F. and Zachara J. M. (1989) Subsurface transport of contaminants. *Environ. Sci. Technol.* **23,** 496–502.

Morel F. M. M. and Hering J. G. (1993) *Principles and Applications of Aquatic Chemistry*. John Wiley, New York.

Myers M. N. and Giddings J. C. (1982) Properties of the transition from normal to steric field-flow fractionation. *Anal. Chem.* **54,** 2284–2289.

Pham M. K. and Garnier J.-M. (1998) Distribution of trace elements associated with dissolved compounds (<0.45 μm-1 nm) in freshwaters using coupled (frontal cascade) ultrafiltration and chromatographic separations. *Environ. Sci. Technol.* **32,** 440–449.

Phillips C. S. G. and Willliams R. J. P. (1966) *Inorganic Chemistry*. Clarendon Press.

Powell R. T., Landing W. M., and Bauer J. E. (1996) Colloidal trace metals, organic carbon and nitrogen in a southeastern U.S. estuary. *Mar. Chem.* **55,** 165–176.

Stumm W. and Morgan J. J. (1996) *Aquatic Chemistry*. John Wiley, New York.

Tanizaki Y., Shimokawa T., and Nakamura M. (1992) Physicochemical speciation of trace elements in river waters by size fractionation. *Environ. Sci. Technol.* **26,** 1433–1444.

Tipping E. (1981) The adsorption of aquatic humic substances by iron oxides. *Geochim. Cosmochim. Acta* **45,** 191–199.

Tipping E. (1994) WHAM—A chemical equilibrium model and computer code for waters, sediments, and soils incorporating a discrete site/electrostatic model of ion-binding by humic substances. *Comput. Geosci.* **20,** 973–1023.

Tipping E (1996) *Information for WHAM Users* [distributed with the WHAM computer programme]. Institute of Freshwater Ecology.

Tipping E. and Hurley M. A. (1992) A unifying model of cation binding by humic substances. *Geochim. Cosmochim. Acta* **56,** 3627–3641.

Turner D. R., Whitfield M., and Dickson A. G. (1981) The equilibrium speciation of dissolved components in freshwater and seawater at 25°C and 1 atmosphere pressure. *Geochim. Cosmochim. Acta* **45,** 855–881.

Varney M. S., Mantoura R. F. C., Whitfield M., Turner D. R., and Riley J. P. (1983) Potentiometric and conformational studies of the acid-base properties of fulvic acid from natural waters. In *Trace Metals in Seawater* (eds. C. S. Wong, E. A. Boyle, K. W. Bruland, J. D. Burton, and E. D. Goldberg), pp. 751–772. Plenum, New York.

Wen L.-S., Santschi P., Gill G., and Paternostro C. (1999) Estuarine trace metal distributions in Galveston Bay: Importance of colloidal forms in the speciation of the dissolved phase. *Mar. Chem.* **63,** 185–212.

Whitfield M. and Turner D. R. (1987) The role of particles in regulating the composition of seawater. In *Aquatic Surface Chemistry* (ed. W. Stumm), pp. 457–493. John Wiley, New York.

Wilkinson K. J., Balnois E., Leppard G. G., and Buffle J. (1999) Characteristic features of the major components of freshwater colloidal organic matter revealed by transmission electron and atomic force microscopy. *Colloids Surf., A* **155,** 287–310.

Vogl J. and Heumann K. G. (1997) Determination of heavy metal complexes with humic substances by HPLC/ICP-MS coupling using on-line isotope dilution technique. *Fresenius J. Anal. Chem.* **359,** 438–441.

Vogl J. and Heumann K. G. (1998) Development of an ICP-IDMS method for dissolved organic carbon determinations and its application to chromatographic fractions of heavy metal complexes with humic substances. *Anal. Chem.* **70,** 2038–2043.